Journal of Membrane Science & Research

MRXUQDO KRPHSDJH ZZZ PVUMRXUQDO FRP

Research Paper

(YDOXDWLRQ RI 9DSRU 'HSRVLWLRQ 7HFKQLTXHV IRU

6DQNHW .HONDU &ROLQ $:ROGHQ

'HSDUWPHQW RI &KHPLFDO %LRORJLFDO (QJLQHHULQJ &RORUDGR 6FKRRO RI 0LQHV *ROG

ARTICLE INFO

Received 2016-05-03
Revised 2016-06-24
Accepted 2016-06-26
Available online 2016-06-26

GRAPHICAL ABSTRACT

KEYWORDS

Asymmetric nanopores
Pulsed PECVD
Physical vapor deposition
Plasma-enhanced atomic layer deposition
Track etched membranes

HIGHLIGHTS

‡ 1DQRSRUH PHPEUDQHV PRGL¿HG E\ 39' $/' DQG SXOVHG 3(&9'
• Feature scale model used to design membranes and analyze performance
• Pulsed PECVD forms asymmetric membranes with nanoscale control
‡ 7KH PHPEUDQHV KDYH KLJK SXUH ZDWHU ÀX[HV DQG JRRG SURWHLQ UHMHFWLRQ

ABSTRACT

7KH VXLWDELOLW\ RI WKUHH YDSRU GHSRVLWLRQ WHFKQLTXHV IRU SRUH VL]H PRGL¿FDWLRQ ZDV HYDO ZDV HPSOR\HG WR SUHGLFW WKH SRUH JHRPHWU\ DIWHU PRGL¿FDWLRQ DQG WKH UHVXOWLQJ SXUH Z GHSRVLWLRQ 3(&9' QDWXUDOO\ IRUP DV\PPHWULF QDQRSRUHV WKDW UHWDLQ KLJK ÀX[DV SRUH VL ,Q FRQWUDVW SXOVHG 3(&9' DQG SODVPD HQKDQFHG DWRPLF OD\HU GHSRVLWLRQ 3($/' ZHUH VKRZQ EHWZHHQ PRGHO SUHGLFWLRQV DQG ÀX[PHDVXUHPHQWV ([SRVXUH OLPLWDWLRQV GXULQJ 3($/' LQWU VPDOOHU WKDQ SXOVHG 3(&9' DQG 39')LOWUDWLRQ H[SHULPHQWV XVLQJ ERYLQH VHUXP DOEXPLQ DV VLPXOWDQHRXVO\ GHOLYHU ERWK KLJK ÀX[DQG KLJK VHOHFWLYLW\ )RU H[DPSOH SXOVHG 3(&9' PRGL RI WKHLU LQLWLDO SXUH ZDWHU ÀX[

‹ 035/ $OO ULJKWV UH

,QWURGXFWLRQ

3RUH VL]H PRGL¿FDWLRQ LV DQ LPSRUWDQW ... selectivity of both polymeric and inorganic membranes [1-3] ... EDVHG WHFKQLTXHV V [4] and electroless gold deposition ... tion [5] KDYH EHHQ HPSOR\HG WR PRGLI\ WKH ... RI PHPEUDQHV 7KHVH PRGL¿FDWLRQ WHFKQLTXHV ... VXPLQJ SURFHVVLQJ VWHSV LQYROYLQJ H[SRVXUH ... LVVXHV OLPLW WKHLU DSSOLFDWLRQ RQ D ... techniques such as chemical vapor deposition (CVD) [6] ... deposition (PVD) [8] DQG DWRPLF OD\HU GHSRVLWLRQ [9,10] are more

ÀH[LEOH DOWHUQDWLYHV IRU SRUH PRGL¿FDWLRQ ... 6ROXWLRQ EH FRQWUROOHG RYHU D ZLGH UDQJH 2Q ... Optimization of these techniques largely relies on empirical studies of per ... micrograph (SEM) images are often used to document the degree of pore closure ... ZLWK WKH RQO\ FRQWURO LV WKH ... DQG HQJLQHHU ¿QDO SRUH VL]H DQG VKDSH IRU

&RUUHVSRQGLQJ DXWKRU DW 3KRQH ID[
E-mail address: FZROGHQ#PLQHV HGX &$:ROGHQ

DOI: 10.22079/jmsr.2016.20345

examine the modification of model supports using different vapor deposition techniques through a combination of experiment and modeling.

Polymeric track-etched (TE) membranes are often used as model supports due to their well-defined size and geometry, and narrow pore size distribution, as well [12, 13]. These membranes are fabricated by bombarding polymeric films with heavy nuclei to create damaged track, which are subsequently etched to create nano-sized pores [14]. Approaches which can tailor the pore size and surface properties of TE membranes would be an enabling innovation for extending the application spectrum of these membranes [10, 15, 16]. For instance, it has been shown that post-modification of polymeric TE membranes can drastically improve their hydrophilicity [17], anti-fouling properties [18] and selectivity [3]. In principle, it should be possible to modify these membranes with a thin selective layer, which shouldn't adversely affect the flux, but drastically improve the selectivity due to reduction in pore size [19].

PVD techniques such as thermal evaporation and sputtering have been commonly used for surface modification [17], as well as for creating catalytic membrane surfaces [20]. The simplicity of this high rate deposition method makes PVD appealing for membrane modification. PVD techniques produce asymmetric nanopores since deposition does not penetrate inside the pores, significantly [8]. Such non-conformal coatings could potentially help overcome the trade-off between maintaining high flux and good selectivity. Here thermal evaporation of aluminum was used as a benchmark for comparing PVD with the other pore size modification techniques described below.

ALD has emerged as a leading approach for precise pore size reduction and surface modification of TE membranes [2, 9, 10, 15]. ALD provides digital control over the thickness due to its self-limiting nature, and the thickness of the material can be tuned precisely by simply varying the number of deposition cycles. In this work, PEALD of titania (TiO_2) was employed as one of the techniques for tailoring pore size of track-etched membrane supports. PEALD is a variation of ALD in which plasma is employed during one of the exposure steps of the ALD cycle to drive the chemistry [21]. The application of plasma allows for the deposition to be carried out at significantly lower temperatures that are compatible with polymeric membrane supports.

Despite its elegant nature, the ALD route for pore size modification has a few drawbacks. First, the conformal nature of ALD leads to densification of the pore interior, which can lead to severe flux reduction [9, 22]. Second, practical application of ALD for coating larger pores could be problematic due to the extremely low growth rates in ALD, which severely limits the throughput. Lastly, it is often assumed that ALD provides perfect conformality throughout the structure, but this requires that both the precursor dose and the purge times be sufficiently large to ensure complete delivery/removal of reactants/products. The original TE membrane supports are very high aspect ratio structures, and the aspect ratio increases dramatically as pore closure is approached [23]. In practice, it is unlikely that sufficient exposure and purge times are used to ensure conformal coverage throughout deposition. This can be advantageous in that exposure-limited ALD process can be exploited in membrane applications to fabricate non-conformal pores for high flux applications. The feature scale modeling tool is applied to analyze the consequences of operating ALD in an exposure-limited mode.

The novel pore modification technique used in this work is pulsed PECVD. Pulsed PECVD is an alternative that provides the throughput and asymmetry of PVD while retaining the digital control offered by ALD. Our group has developed pulsed PECVD as an alternative to ALD for digital control over deposition on planar surfaces for a number of oxides including SiO_2 [24], TiO_2 [25], Al_2O_3 [26], and ZnO [27]. In this technique a metal precursor highly diluted in oxygen is continuously delivered to the reactor and the plasma is pulsed using square wave modulation at low frequency (~1 Hz). Under appropriate conditions, pulsed PECVD can be operated in a self-limiting fashion. First, it requires that no thermal CVD occurs when the plasma is off. This condition is met because molecular oxygen is unreactive with many precursors, such as $TiCl_4$ at low temperature. The second requirement is that no deposition occurs under continuous plasma operation. This occurs when the diluted precursor is fully consumed or sacrificially deposited before it can reach the substrate [28]. So while no deposition occurs when the plasma is continuously off or on, under pulsed operation at low frequency (~1 Hz) deposition is readily observed, and the growth per cycle can be adjusted over a reasonable range (0.5 – 5 Å/pulse) through control of parameters such as precursor flowrate and duty cycle. The elimination of purge steps leads to higher net deposition rates [29], while the use of plasma enables high quality metal oxides to be deposited at temperatures compatible with polymeric substrates [30].

In the present work, PVD, PEALD and pulsed PECVD were evaluated for pore size and shape modification of TE membranes having a nominal pore opening of ~100 nm. SEM imaging was employed to investigate the pore opening and surface morphology of the coated pores. A feature scale model is used to design pore geometries and predict their performance. The model is validated by experimental measurement of flux and selectivity for membranes modified by the three different vapor deposition techniques. Membrane performance was evaluated using measurements of pure water flux and solute rejection through these modified supports using a stirred cell ultrafiltration apparatus.

1. Experimental

2.1. Materials

Commercial polycarbonate track-etched membranes, known as Isopore™, were purchased from EMD Millipore Corporation. Figure 1 displays top view and cross sectional micrographs of the hydrophilic pristine support. The support openings are tightly distributed around the nominal 100 nm (± 3 nm) pore size, but a few "doublets" are also present where two pores have fused together. These doublets account for ~7.5% of the total number of pores in the supplied membrane filter. The cross-section image shows the vertical alignment of the features extending throughout the nominal 25 µm thick support.

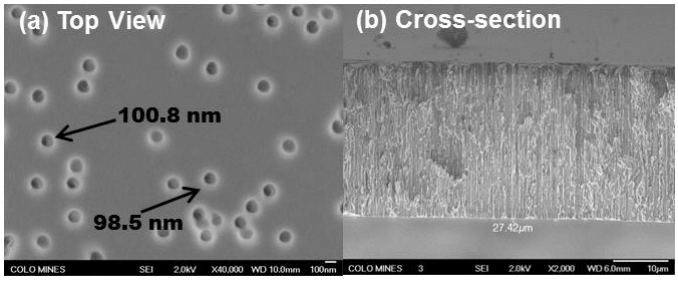

Fig. 1. (a) Top view and (b) cross-section SEM micrographs of uncoated TE membrane supports.

Titanium tetrachloride (99% pure) was purchased from Sigma Aldrich, and used as a precursor in pulsed PECVD and PEALD modifications. Ultrahigh purity grade argon and oxygen were used as the carrier gas and oxidant, respectively. Bovine serum albumin (BSA, molecular weight 66 kDa, Sigma Aldrich) was used to test the separation efficiency of the pristine and modified membranes.

2.2. Membrane fabrication

Pristine TE membranes were modified using 3 deposition techniques, including PVD of aluminum, PEALD and pulsed PECVD of Titania. Aluminum evaporation was chosen for its simplicity while Titania was chosen for a number of reasons. It is a stable material that may be easily functionalized, and it is commonly used for membrane modification [31]. In addition, it maintains a hydrophilic surface [10], so that the changes in membrane performance observed in this work should be primarily due to geometrical effects and not due to changes in surface energetics. Thermal evaporation of aluminum onto TE membranes was performed in a diffusion-pumped bell jar with a base pressure of 10^{-7} torr. The membranes were positioned at normal incidence to the evaporation boat, and a shutter and quartz crystal microbalance were used to control the thickness of the aluminum coating. Pulsed PECVD and PEALD of TiO_2 was performed in a capacitively coupled plasma reactor described previously [25]. The samples were mounted to the grounded electrode which was resistively heated to 70 °C, well below the maximum operating temperature of the polycarbonate TE membranes used in this study. During pulsed PECVD operation, titanium tetrachloride, Ar diluent, and O_2 were supplied continuously in the reactor without the need of any intermediate purge steps as described, previously [25]. The precursor was stored in a temperature-controlled bubbler at T = 15 °C, and delivered using Ar as the carrier gas. The plasma power was 50 W, and a square wave modulation was applied to plasma power using a LabVIEW program. The duration of on and off times was 0.5 s each, and the resulting TiO_2 growth per cycle (GPC) was 1.2 Å/pulse. During PEALD operation, the process parameters like plasma power, substrate temperature and gas flow rates were kept the same as in the pulsed PECVD process. The oxygen and diluent argon were flown continuously in the reactor, serving as the purge gas. The precursor flow was alternately directed to the reactor or

directly to the vacuum pump through the LabVIEW-controlled solenoid valves. For modification of TE membranes, the PEALD process employed 17 s purges, a $TiCl_4$ dose time of 8 s, and 6 s of plasma exposure. The desired degree of pore closure in PEALD and pulsed PECVD was achieved by varying the number of deposition cycles.

2.3. Membrane characterization

Variable angle spectroscopic ellipsometry (VASE, J. A. Woollam WVASE32) was employed to measure the thickness of the pulsed PECVD and PEALD TiO_2 coatings, whereas the thickness of the Al coating was determined using profilometry. Field emission scanning electron microscopy (FESEM) (JEOL JSM-7000 F) was used to study the surface morphology of the modified TE membranes. PEALD- and pulsed PECVD- modified TE membranes were sputter-coated with a thin layer of gold before FESEM imaging to reduce charging, whereas no such coating was required for the Al-coated samples. The pure water flux of PVD-, PEALD-, and pulsed PECVD-modified TE membranes was measured using a stirred ultrafiltration cell (Amicon, Millipore Co.) under 10 psi overhead pressure, and the resulting flux is reported normalized to the flux of unmodified TE membranes. BSA was used to determine the solute rejection using a 1 g/L solution prepared in a phosphate buffered saline to maintain the pH at 7.4. During solute rejection measurements, the retentate solution was continuously stirred at 400 rpm using a magnetic stirrer. The concentration of BSA in the filtrate was determined by measuring the absorbance values at 280 nm with a Cary 5G UV-Vis-NIR spectrophotometer.

3. Design and analysis of asymmetric pores

Transport properties of nanopores are closely linked to their geometry. As mentioned earlier, the use of plan view microscopy to characterize the pore size of modified membranes can have limitations. This is illustrated in Figure 2, which compares a plan view micrograph, a cross-section micrograph, and a feature scale simulation of silicon wafers patterned with ~125 nm contact holes and modified by pulsed PECVD of alumina. Patterned wafers were used as surrogates to enable cross-sectional imaging, which is very difficult to achieve from polymeric TE supports. The plan view image (see Figure 2a) suggests that the average pore opening is ~ 30 nm. However, the cross-sectional image of the nanopore (see Figure 2b) reveals that the minimum pore opening is much smaller, approximately 10 nm. When these pores are coated there is significant curvature as the pore is closed, and with plan view imaging it is difficult, if not impossible, to focus on the position of the minimum pore opening.

In order to engineer the membrane performance, it is imperative to be able to predict the geometry of the modified pores. Though seldom applied in membrane modification, the microelectronics community has employed feature scale models for decades to understand and control the deposition of films on non-planar substrates [32-35]. Recently, we developed a feature scale model that can be used to simulate PVD, ALD, and the transient growth modes that contribute to deposition in pulsed PECVD [36]. The model employs a diffusion reaction framework, in which steady state deposition is modeled based on surface reaction probability (γ), with PVD (γ =1) and ALD (γ→0) representing the two limits.

Pulsed PECVD is a transient deposition process that involves two growth modes as discussed previously [28]. The first growth mode is analogous to ALD. During the plasma off state, the precursor adsorbs on the substrate surface, and these adsorbed molecules then react with oxygen radicals during the plasma on step to contribute to conformal film growth. The second growth mode is due to reactive species that are formed at plasma ignition, and then deposit with near unity sticking probability (γ =1) in a manner analogous to PVD. To capture the two growth modes of pulsed PECVD, the model simply alternates between conditions used to simulate ALD and PVD, using the single adjustable parameter '*R*', which is the ratio of the PVD growth component to the ALD growth component. This value can be determined experimentally using the GPC values measured for both PEALD and pulsed PECVD. For example, if the PEALD GPC is 1 Å/cycle and the pulsed PECVD rate is 2 Å/cycle then R = 1, which means there are equal contributions from both growth modes. This model has been validated for both cylindrical pores and Cartesian trenches, with Fig. 2c providing further validation of its capabilities. The nanopore geometries predicted by the feature scale model are then employed to predict pure water flux using COMSOL by solving the Navier-Stokes equations for pressure driven flow.

Precursor diffusion limitations can occur while coating very high aspect ratio features. The feature scale model utilized in this work accounts for exposure limitations that can limit the extent of deposition in high aspect ratio features in both ALD and pulsed PECVD. For a given precursor exposure, there is a critical aspect ratio (a*) that can be coated conformally during ALD, and its value can be determined from the scaling relationships developed by Gordon and co-workers [23]. In the model, the local aspect ratio (a(z, t)) is calculated as deposition proceeds, and once the local aspect ratio exceeds a*, no further ALD growth is allowed at that position.

One utility of this model is that it can be used to design and analyze the performance of membrane supports modified by vapor deposition. Fig. 3 compares simulated profiles of 100 nm diameter nanopores modified by ALD, pulsed PECVD at R = 1, and PVD. The white area represents the material deposited, whereas the black region represents the surrounding gas phase. These simulations were performed using cylindrical pores with an initial opening of 100 nm, and in each case deposition was allowed to proceed until the minimum pore opening was reduced to 20 nm. Fig. 3a shows an ALD-modified pore assuming no exposure limitations, which is perfectly conformal and results in densification of the underlying support. The other extreme, Fig. 3c, shows the feature predicted for an ideal PVD process with unity sticking coefficient. Very little deposition is observed within the feature, creating a highly asymmetric pore structure that would be ideal for membrane applications. A drawback of this technique is that it requires considerably more deposition to achieve the same degree of pore closure. Finally, Fig. 3b shows the simulation for pulsed PECVD at R = 1, in which the contributions of the two growth modes are equal. The pore closure is asymmetric reflecting the benefits of PVD, but the total amount of material required is closer to the ALD case.

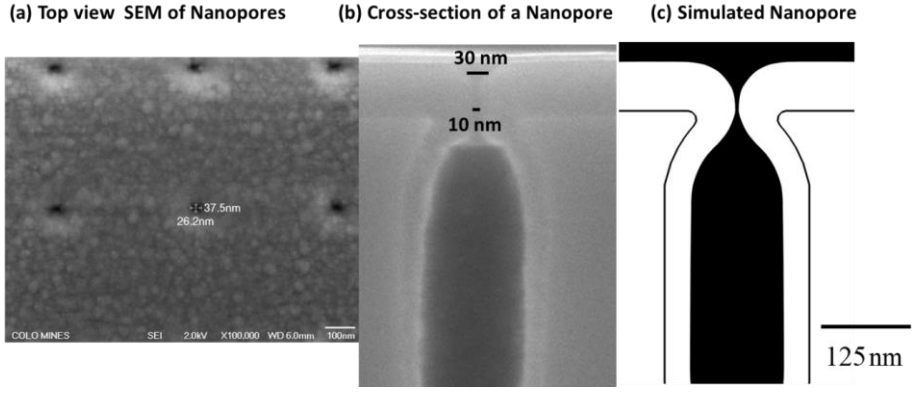

Fig. 2. (a) Top view SEM micrograph of nanopores fabricated using pulsed PECVD; (b) Cross-section SEM of a nanopore; (c) model prediction of the nanopore geometry using the simulation procedure described in this work.

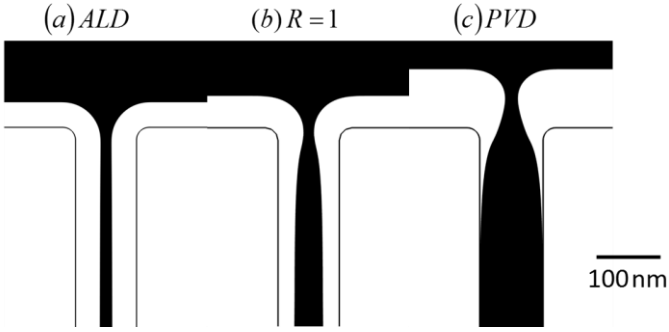

Fig. 3. Simulated deposition profiles on 100 nm features coated by (a) ALD, (b) pulsed PECVD, and (c) PVD for a final pore opening of 20 nm.

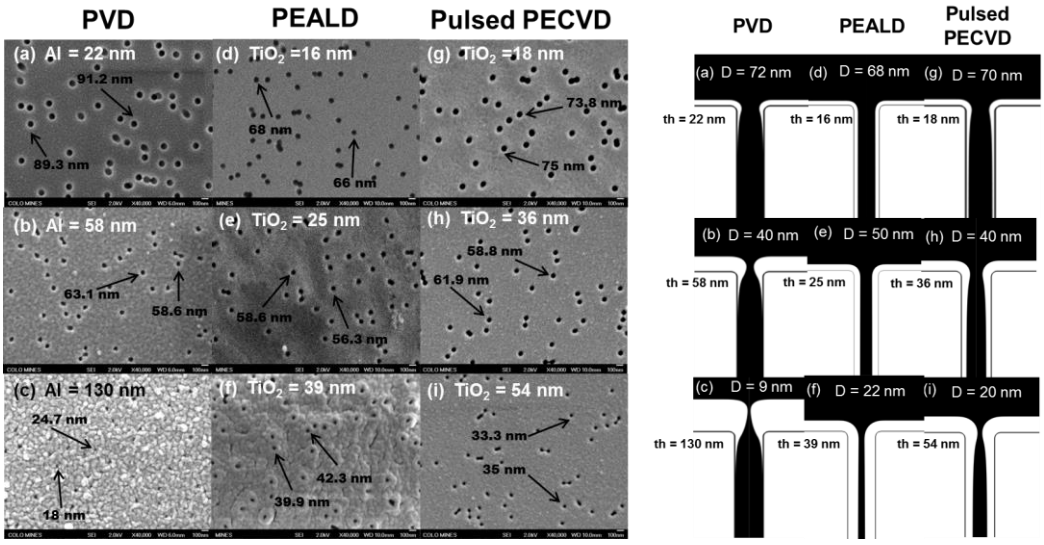

Fig. 4. The left panel displays top view micrographs of TE membranes modified by PVD of aluminum (a-c), PEALD of TiO2 (d-f), and pulsed PECVD of TiO2 (g-i) as a function of planar film thickness. The right panel displays the corresponding feature scale simulation of the resulting geometries noting the minimum pore diameter for these 9 cases.

In the results below, the feature scale model is used to simulate the nanopore geometries formed by vapor deposition on 100 nm diameter isopore supports. Membranes coated by aluminum evaporation employed the PVD simulation described above. The pore geometry of the TE membranes modified by PEALD was simulated by superimposing precursor diffusion limitations on the ideal ALD case shown in Fig. 3a. The critical aspect ratio during these depositions was estimated to be around a* = 36, based on the 8 s $TiCl_4$ exposure. This means that deposition initially extends ~3.6 µm into the 25 µm pore, and this depth will continue to decrease as the pore shrinks.

The model parameters for pulsed PECVD reflected the experimental conditions. Based on the $TiCl_4$ exposure provided during the ½ second plasma off step, a critical aspect ratio of a*= 8.2 was estimated. Again, this implies that initially the ALD growth component extends 820 nm into the pore, and this value diminishes as growth proceeds. Note that this value of a* represents an upper limit, and the simulations were not significantly sensitive to this parameter. Using identical precursor doses the measured GPC for PEALD and pulsed PECVD were 0.56 Å/cycle and 1.2 Å/cycle, respectively. Hence, the corresponding PVD/ALD ratio or *R* was determined to be ~1. The net planar growth rate in pulsed PECVD was 7.2 nm/min, over 35 times faster than the 0.2 nm/min obtained with the PEALD process.

4. Results and discussion

The left panel of Figure 4 shows the top view SEM micrographs of TE membranes modified by different vapor deposition techniques employed in this work as a function of thickness. The labels report the planar thickness of the deposited film, and the arrows in the micrographs point out the apparent diameter of the resulting pore openings. The right panel of Fig. 4 displays simulated cross-sections of the resulting pore geometries at these same conditions, and the labels indicate the minimum pore diameter under these conditions. The specific conditions were chosen to provide examples of low, intermediate, and high degrees of pore closure for each deposition technique.

There are a number of important observations to take away from this figure. First, the micrographs confirm that the amount of deposited material required to achieve the same degree of pore closure varies by techniques in the descending order of PVD > pulsed PECVD > PEALD, as predicted in Fig. 3. For example, to reduce the minimum pore diameter to 40 nm requires 30 nm of deposition by PEALD, 36 nm of pulsed PECVD, and 58 nm of PVD. Moreover, the differences become more pronounced as the degree of pore closure increases. Second, this figure confirms the limitations of using top view microscopy for evaluation of pore closure. At low levels of deposition (see Figure 4a/d/g), the pore diameter estimated from SEM images is in good agreement with model predictions. However, the disparity between these values gets worst with increasing deposition. At a high degree of pore closure (see Figure 4c/f/i) the SEM image overestimates the minimum pore size by a factor of ~2 for all three deposition techniques. Finally, it is observed that the morphology of the three films are quite different. In the case of evaporated aluminum, the coatings are rough, reflecting the Volmer–Weber growth mode that results in a polycrystalline morphology [37]. These films would fall into zone 1 of the Thornton diagram [38], which consists of columnar growth with voided defects due to atomic shadowing. The diffusion-reaction model does not capture these features, but as shown below it has a significant impact on membrane performance.

At low deposition thickness, both pulsed PECVD and PEALD display a smooth surface morphology. However, at a coating thicknesses > 30 nm the PEALD becomes rough and appears to become polycrystalline (see Fig. 4f), whereas the pulsed PECVD film remains smooth and amorphous. This behavior reflects the unique feature of TiO_2. It has been observed that ALD initially produces amorphous TiO_2, but there is a critical thickness at which point the film transforms into the polycrystalline anatase phase. The exact value of this transition depends on deposition conditions [39-41]. Due to its slower growth rate, the PEALD films likely have better quality and transform from amorphous to polycrystalline at a lower thickness than the pulsed PECVD films.

Figure 5 compares the membrane flux as a function of the planar

thickness for the three different modification methods. As could be observed, uncoated supports had a pure water flux (PWF) of 7360±294 L/(m^2.h.bar). Relative flux is defined as the pure water flux (PWF) of a coated TE membrane normalized with respect to that of the uncoated TE membranes. The solid black lines represent the flux predicted by the feature scale model, which were obtained by exporting the simulated geometries of the modified pores into another COMSOL module and modeling Hagen-Poiseuille flow through the resulting pores. In addition, the flux expected from a perfectly conformal coated pore is included as the dashed red lines for comparison. The flux of a conformally coated membrane is predicted to drop, sharply, due to densification of the pores. In contrast, the techniques used in this work that lead to asymmetric pore closure allow the flux to remain largely unchanged until the pore diameter is reduced <20 nm.

Figure 5a shows the results for the PVD-modified membrane. There is generally good agreement between the measured and predicted flux. However, there is significant scatter in the data and poor reproducibility, which is attributed to the roughness and morphological instabilities associated with the columnar growth mode discussed above. As expected, the asymmetric pore geometry allows the flux of PVD-modified supports to remain nominally unchanged up to a thickness of 75 nm. The flux of the membranes drops to 0 only for coating thicknesses >125 nm. In the range of 75 -125 nm, where pore closure is approached, there is great variability with similarly coated pores delivering high flux or no flux. This makes PVD unsuitable for nanoscale control of performance.

In contrast, both PEALD and pulsed PECVD provided excellent reproducibility and control over the degree of pore closure. In the case of PEALD (see Figure 5b), the flux declines approximately linearly with the amount of TiO_2 deposited, and the agreement with the model is excellent. The measured flux is slightly greater than model predictions in the transition regime, and there is a very small but non-negligible flow measured for membrane modified with >50 nm of material, where pore closure is predicted. Both of these minor deviations are attributed to the presence of the doublets (see Figure 1a) that are not accounted for in the model. The stark contrast between the conformal prediction and the observed performance highlights the importance of operating ALD in the exposure limited regime in order to maintain significant flux.

Pulsed PECVD (see Figure 5c) combines the asymmetry of the PVD modification with the control and reproducibility of ALD. The flux is unchanged up to 30 nm of deposited material, and then it begins to attenuate as pore closure is reached. The flux drop off in this regime is steep, and the digital control and smooth morphology enables precise control over membrane properties. The amount of material for complete pore closure is just slightly greater than PEALD, but less than half the material required by PVD. For all three deposition techniques, the experimentally measured flux is well captured by the model, validating its utility for this application.

The selectivity of the modified membranes was evaluated using bovine serum albumin (BSA) as a model solute in a stirred ultrafiltration cell. These results were not significantly impacted by protein adsorption as it was found that both the pristine TE membranes and all of the modified supports exhibited excellent anti-fouling characteristics. The membranes exhibited a static BSA adsorption value <10 µg/cm^2 after immersion in a 1 g/L BSA solution for 24 hours. This is attributed to the hydrophilic nature of the original TE membranes.

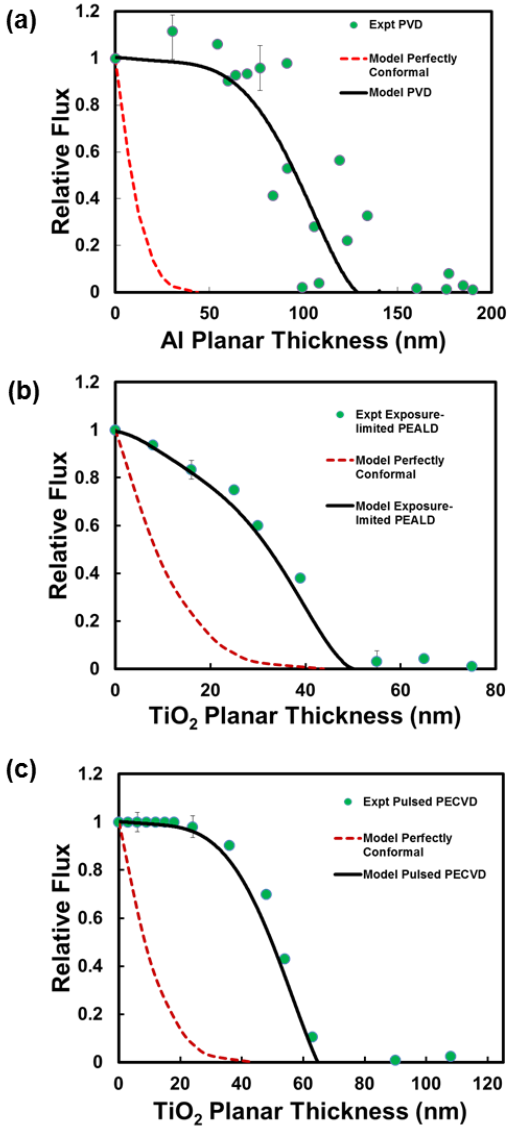

Fig. 5. Comparison of experimentally measured (points) and predicted flux (black lines) as a function of deposition thickness for TE membranes modified by (a) aluminum PVD, (b) PEALD of titania, and (c) pulsed PECVD of titania. The dashed red line is the prediction for perfectly conformal modification.

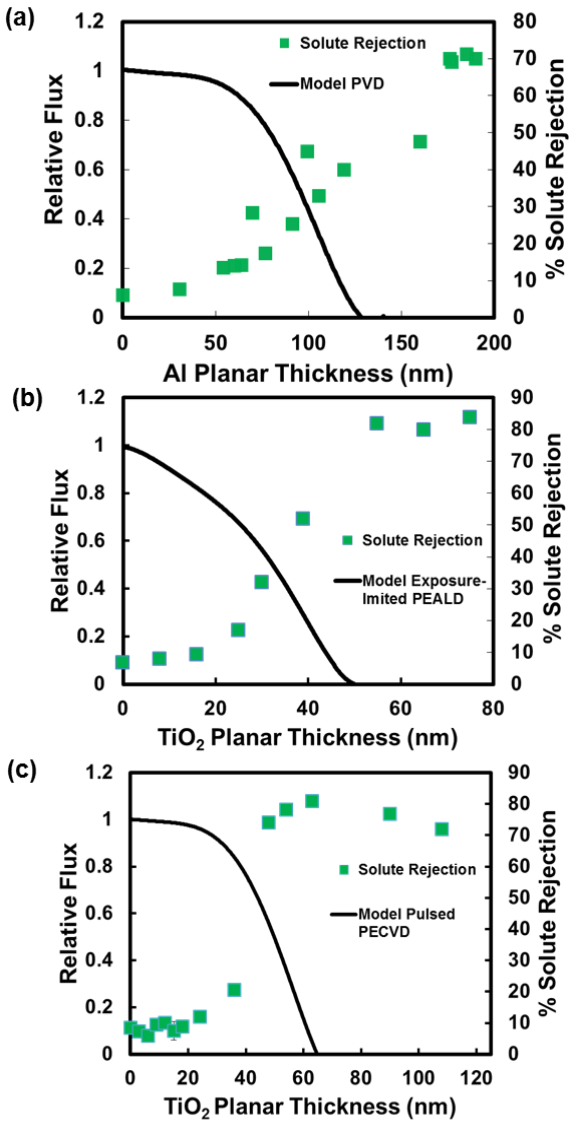

Fig. 6. Solute rejection and predicted flux as a function of film thickness for (a) PVD-modified membranes; (b) PEALD-modified membranes and (c) Pulsed PECVD-modified membranes. Circled values indicate membranes that displayed the best combination of flux and selectivity for each technique as discussed in the text.

The hydrophilicity, and hence the anti-fouling nature, of the membranes is maintained even after modification. Hydrophilicity of the membranes was tracked using a simple home-made contact angle measurement apparatus [42]. The contact angle of the pristine TE membranes, TiO_2-modified membranes, and Al-modified membranes were 44±3°, 52±5°, and 65±7°, respectively. It should be noted that the TiO_2-modified TE membranes were initially very hydrophilic ($\theta \sim 0°$). However, the hydrophilicity is quickly lost upon exposure to the atmosphere due to hydrocarbon contamination.

Figure 6 compares the solute rejection and the modeled flux of the modified TE membranes as a function of the planar thickness of the deposited coatings. BSA (molecular size ~ 7 nm) was used as the model solute. Figure 6a displays the solute rejection of the PVD-modified supports. Solute rejection scales linearly with thickness, and reaches a maximum of ~70% only after the evaporation of 200 nm of aluminum, at which point the flux is negligible. As with measurement of flux, the solute rejection data is also very noisy, reflecting the rough morphology of these layers. The optimal value for PVD modification was achieved at 100 nm of coating thickness. In this membrane, the solute rejection was just 44%, and though the model predicts 45% of the original flux the measured value was just 29%. With the PVD-modified supports >50% solute rejection was only achieved when the flux approaches zero.

In the case of PEALD, the solute rejection was negligible (<10 %) and unchanged through 20 nm of deposition. The rejection then increases linearly between 20 and 50 nm, where the rejection saturates at ~80%. At this point, the 100 nm pores are completely closed, and the remaining flux of BSA solutes is due to doublets. Optimal performance was achieved with the membrane coated with 39 nm of TiO_2 film. At this point, the 50% solute rejection was achieved while retaining 40% of the initial membrane flux. So, although the control and reproducibility was significantly improved relative to PVD modification, only modest improvements in selectivity/flux were obtained.

In contrast to PEALD, the retention behavior of membranes modified by pulsed PECVD exhibit step function behavior as shown in Fig. 6c. For <25 nm of TiO_2 deposition, the membranes display negligible solute rejection (~7%) that is unchanged from the uncoated support. The rejection level increases sharply between 40-50 nm of deposited material to a value of ~75%, that remains essentially unchanged with additional coating and is attributed to the presence of doublets. The membrane modified by 48 nm of TiO_2 deposition retained ~70% of the original flux, and the BSA solute rejection approaches the saturation threshold (~ 75%). This is a tremendous improvement over both PVD and PEALD modification. The window for optimal performance is narrow, and thus the digital control over deposition provided by pulsed PECVD is important in achieving this level of performance.

5. Conclusions

Track-etched membrane supports were modified using PVD of aluminum, PEALD and pulsed PECVD of Titania. A feature scale model was used to design the resulting pore geometries, successfully predicting the flux behavior of modified membranes. PVD modification results created highly asymmetric nanopores that in principle should lead to high flux and good selectivity. However, PVD requires much more material for comparable pore

closure, and the rough, columnar growth morphology limits reproducibility and solute retention. PEALD was shown to deliver precise pore size reduction, requiring significantly less film deposition in comparison to PVD. By operating in a precursor exposure limited regime, the PEALD-modified membranes exhibited higher flux than would be achieved with perfectly conformal deposition. However, both flux and retention scale linearly with deposition thickness, limiting the ability to simultaneously optimize both quantities. Pulsed PECVD produced asymmetric pores characteristic of PVD while displaying the precision and reproducibility of PEALD. Both flux and retention display step function behavior with respect to thickness, creating a small window to overcome the flux/selectivity tradeoff. The digital control of pulsed PECVD enabled access to this region, achieving maximum solute rejection while retaining 70% of the original flux.

6. Acknowledgements

The authors gratefully acknowledge the financial support from the National Science Foundation through award CBET-1033203.

7. References

[1] M. Pan, C. Cooper, Y.S. Lin, G.Y. Meng, CVD modification and vapor gas separation properties of nanoporous alumina membranes, J. Membr. Sci. 158 (1999) 235-241.
[2] F. Li, Y. Yang, Y. Fan, W. Xing, Y. Wang, Modification of ceramic membranes for pore structure tailoring: The atomic layer deposition route, J. Membr. Sci. 397 (2012) 17-23.
[3] A. Asatekin, K.K. Gleason, Polymeric nanopore membranes for hydrophobicity-based separations by conformal initiated chemical vapor deposition, Nano Lett. 11 (2011) 677-686.
[4] T. Ito, T. Hioki, T. Yamaguchi, T. Shinbo, S.-I. Nakao, S. Kimura, Development of a molecular recognition ion gating membrane and estimation of its pore size control, J. Am. Chem. Soc. 124 (2002) 7840-7846.
[5] K.B. Jirage, J.C. Hulteen, C.R. Martin, Nanotubule-based molecular-filtration membranes, Science 278 (1997) 655-658.
[6] Y.-Y. Li, T. Nomura, A. Sakoda, M. Suzuki, Fabrication of carbon coated ceramic membranes by pyrolysis of methane using a modified chemical vapor deposition apparatus, J. Membr. Sci. 197 (2002) 23-35.
[7] S. Araki, N. Mohri, Y. Yoshimitsu, Y. Miyake, Synthesis, characterization and gas permeation properties of a silica membrane prepared by high-pressure chemical vapor deposition, J. Membr. Sci. 290 (2007) 138-145.
[8] K. Grigoras, V.-M. Airaksinen, S. Franssila, Coating of nanoporous membranes: atomic layer deposition versus sputtering, J. Nanoscience Nanotechnol. 9 (2009) 3763-3770.
[9] F. Li, L. Li, X. Liao, Y. Wang, Precise pore size tuning and surface modifications of polymeric membranes using the atomic layer deposition technique, J. Membr. Sci. 385 (2011) 1-9.
[10] Q. Wang, X. Wang, Z. Wang, J. Huang, Y. Wang, PVDF membranes with simultaneously enhanced permeability and selectivity by breaking the tradeoff effect via atomic layer deposition of TiO_2, J. Membr. Sci. 442 (2013) 57-64.
[11] A.W. Ott, J.W. Klaus, J.M. Johnson, S.M. George, K.C. McCarley, J.D. Way, Modification of porous alumina membranes using Al_2O_3 atomic layer controlled deposition, Chem. Mater. 9 (1997) 707-714.
[12] W. Deen, Hindered transport of large molecules in liquid-filled pores, AIChE J. 33 (1987) 1409-1425.
[13] W. Deen, M. Bohrer, N. Epstein, Effects of molecular size and configuration on diffusion in microporous membranes, AIChE J. 27 (1981) 952-959.
[14] P. Apel, Track etching technique in membrane technology, Rad. Meas. 34 (2001) 559-566.
[15] Q. Xu, J. Yang, J. Dai, Y. Yang, X. Chen, Y. Wang, Hydrophilization of porous polypropylene membranes by atomic layer deposition of TiO_2 for simultaneously improved permeability and selectivity, J. Membr. Sci. 448 (2013) 215-222.
[16] K.C. Khulbe, C. Feng, T. Matsuura, The art of surface modification of synthetic polymeric membranes, J. Appl. Polymer. Sci. 115 (2010) 855-895.
[17] M. Tavakolmoghadam, T. Mohammadi, M. Hemmati, F. Naeimpour, Surface modification of PVDF membranes by sputtered TiO_2: fouling reduction potential in membrane bioreactors, Desal. Water Treat. (2014) 1-11.
[18] C.Y. Tang, Y.-N. Kwon, J.O. Leckie, Effect of membrane chemistry and coating layer on physiochemical properties of thin film composite polyamide RO and NF membranes: II. Membrane physiochemical properties and their dependence on polyamide and coating layers, Desalination 242 (2009) 168-182.
[19] M. Ulbricht, Advanced functional polymer membranes, Polymer 47 (2006) 2217-2262.
[20] S. Cha, W. Lee, Performance of proton exchange membrane fuel cell electrodes prepared by direct deposition of ultrathin platinum on the membrane surface, J. Electrochem. Soc. 146 (1999) 4055-4060.
[21] H.B. Profijt, S.E. Potts, M.C.M. van de Sanden, W.M.M. Kessels, Plasma-assisted atomic layer deposition: Basics, opportunities, and challenges, J. Vac. Sci. Technol. A 29 (2011) 050801.
[22] B.A. McCool, W.J. Desisto, Self-limited pore size reduction of mesoporous silica membranes via pyridine-catalyzed silicon dioxide ALD, Chem. Vap. Deposit. 10 (2004) 190-194.
[23] R.G. Gordon, D. Hausmann, E. Kim, J. Shepard, A kinetic model for step coverage by atomic layer deposition in narrow holes or trenches, Chem. Vap. Deposit. 9 (2003) 73-78.
[24] P.C. Rowlette, M. Canon, C.A. Wolden, Digital control of SiO_2 film deposition at room remperature, J. Phys. Chem. C 113 (2009) 6906-6909.
[25] N.G. Kubala, P.C. Rowlette, C.A. Wolden, Self-limiting deposition of anatase TiO_2 at low temperature by pulsed PECVD, Electrochem. Solid-State Lett. 12 (2009) H259-H262.
[26] S.F. Szymanski, P. Rowlette, C.A. Wolden, Self-limiting deposition of aluminum oxide thin films by pulsed plasma-enhanced chemical vapor deposition, J. Vac. Sci. Technol. A 26 (2008) 1079-1084.
[27] P.C. Rowlette, C.G. Allen, O.B. Bromley, C.A. Wolden, Self-limiting deposition of semiconducting ZnO by pulsed plasma-enhanced chemical vapor deposition, J. Vac. Sci. Technol. A 27 (2009) 761-766.
[28] M.T. Seman, D.N. Richards, P. Rowlette, C.A. Wolden, An analysis of the deposition mechanisms involved during self-limiting growth of aluminum oxide by pulsed PECVD, Chem. Vap. Deposit. 14 (2008) 296-302.
[29] M.T. Seman, D.N. Richards, P.C. Rowlette, N.G. Kubala, C.A. Wolden, Enhancement of metal oxide deposition rate and quality using pulsed plasma-enhanced chemical vapor deposition at low frequency, J. Vac. Sci. Technol. A 26 (2008) 1213-1217.
[30] R.P. Patel, C.A. Wolden, Defect analysis and mechanical performance of plasma-deposited thin films on flexible polycarbonate substrates, Appl. Surf. Sci. 268 (2013) 416-424.
[31] Y. Jun, H. Zarrin, M. Fowler, Z. Chen, Functionalized titania nanotube composite membranes for high temperature proton exchange membrane fuel cells, Int. J. Hydrogen Energy 36 (2011) 6073-6081.
[32] S. Ganguli, S.P. Costello, W.N. Gill, Theory of free boundary step coverage in chemical vapor deposition, Ind. Eng. Chem. Res. 34 (1995) 3380-3391.
[33] M.K. Jain, T.S. Cale, T.H. Gandy, Comparison of LPCVD film conformalities predicted by ballistic transport-reaction and continuum diffusion-reaction models, J. Electrochem. Soc. 140 (1993) 242-247.
[34] T. Cale, T. Gandy, G. Raupp, A fundamental feature scale model for low pressure deposition processes, J. Vac. Sci. Technol. A 9 (1991) 524-529.
[35] M. Cooke, G. Harris, Monte Carlo simulation of thin-film deposition in a rectangular groove, J. Vac. Sci. Technol. A 7 (1989) 3217-3221.
[36] S.S. Kelkar, C.A. Wolden, Feature scale modeling of pulsed plasma-enhanced chemical vapor deposition, J. Vac. Sci. Technol. B 32 (2014) 052001.
[37] S.C. Seel, C.V. Thompson, S.J. Hearne, J.A. Floro, Tensile stress evolution during deposition of Volmer–Weber thin films, J. Appl. Phys. 88 (2000) 7079-7088.
[38] J.A. Thornton, The microstructure of sputter-deposited coatings, J. Vac. Sci. Technol. A 4 (1986) 3059-3065.
[39] H.-E. Cheng, C.-C. Chen, Morphological and photoelectrochemical properties of ALD TiO_2 films, J. Electrochem. Soc. 155 (2008) D604-D607.
[40] M. Ritala, M. Leskelä, E. Nykänen, P. Soininen, L. Niinistö, Growth of titanium dioxide thin films by atomic layer epitaxy, Thin Solid Films 225 (1993) 288-295.
[41] N.G. Kubala, P.C. Rowlette, C.A. Wolden, Self-limiting deposition of anatase TiO_2 at low temperature by pulsed PECVD, Electrochem. Solid-State Lett. 12 (2009) H259-H262.
[42] S.S. Kelkar, D. Chiavetta, C.A. Wolden, Formation of octadecyltrichlorosilane (OTS) self-assembled monolayers on amorphous alumina, Appl. Surf. Sci. 282 (2013) 291-296.